Design of a Wind Tunnel Apparatus to assist Flow and Aeroelastic Control via Zero Net Mass Flow Actuators

Keegan S. O'Donnell[*], Piergiovanni Marzocca[††], Attilio Milanese[¥]
Charles McNall[†], Ratneshwar Jha[§], Erik M. Bollt[¶]

Clarkson University, Potsdam, NY, 13699

Abstract

A plunging-pitching aeroelastic apparatus has been developed to experimentally test new devices for flow and aeroelastic control. The purpose of the experiment is twofold: i) the first phase investigates the aeroelastic behavior of a two-dimensional wing section in post-flutter region, structurally and aerodynamically characterizing the aeroelastic model; ii) the subsequent experiment will be instrumental to test active flow control devices in both the pre- and post-flutter regimes. The design of the testing apparatus utilizes a linear and non-linear cam spring system that allows testing at selected aeroelastic and flowfield conditions. The wing section is mounted to the aeroelastic test apparatus and tests have been conducted in the low speed Clarkson University Wind Tunnel Facility. Plunging and pitching accelerations of the wing during aeroelastic response have been recorded to study and compare the experimental results with the proposed mathematical models. Active flow control devices are bench tested and will be installed in a composite NACA 0018 airfoil at specified locations along the wing span. Zero net mass flow actuators (ZNMF) are considered in this research: ZNMF control devices, such as synthetic jets actuators (SJA) and frequency driven voice coils, are under investigation to demonstrate their ability to actively change the flowfield for improved aeroelastic wing performances. Numerical simulations have already demonstrated improved performance regarding flow and aeroelastic characteristics due to active flow control. Experimental investigation, numerical studies, and corresponding analytical models are provided and pertinent conclusions are discussed.

Nomenclature

a	=	Nondimensional elastic axis location
ab	=	Location of the elastic axis from the middle chord
α	=	Pitching displacement
b	=	Mid-chord
c_h	=	Plunging damping coefficient
c_α	=	Pitching damping coefficient
L	=	Aerodynamic lifting force
L_c	=	Aerodynamic lifting force due to SJA
L_d	=	Aerodynamic disturbance
h	=	Plunging displacement
I_α	=	Total pitching inertia
k_α	=	Torsional spring stiffness

[*] Graduate Research Assistant, Mechanical and Aeronautical Engineering Department, Member AIAA
[††] Assistant Professor, Mechanical and Aeronautical Engineering Department, Member AIAA.
[¥] Graduate Research Assistant, Mechanical and Aeronautical Engineering Department, Member AIAA
[†] Undergraduate Student, Mechanical and Aeronautical Engineering Department
[§] Associate Professor, Mechanical and Aeronautical Engineering Department, Associate Fellow AIAA
[¶] Professor, Mathematics and Computer Science Department

k_h	=	Plunging spring stiffness
m_w	=	Total wing mass
M	=	Aerodynamic moment about the elastic axis
M_c	=	Aerodynamic moment due to SJA
M_d	=	Aerodynamic disturbance
m_c	=	Pitch cam mass
m_T	=	Total plunging mass
s	=	Wing span
t	=	Time
U_∞	=	Free stream velocity

I. Introduction

Aeroelastic induced responses occur due to the interaction of aerodynamic, inertial and elastic forces. Certain aeroelastic instabilities, such as flutter, can jeopardize lifting surfaces performance and survivability [1]. In the safe flight envelope the natural modes (e.g. bending and torsion of lifting surfaces) do not interact. The linear flutter boundary velocity corresponds to a coalescence of two modes and marks the onset of aeroelastic instabilities, leading in extreme cases to catastrophic failures. Due to inherent structural and aerodynamic nonlinearities, the flutter behavior often appears in form of stable constant amplitude oscillations, known in literature as limit cycle oscillations (LCOs). Depending on the nonlinearities of the system and the flight operating conditions LCOs can show a wide range of amplitudes and frequencies. The characteristics of this phenomenon can be reduced to a simplified two degrees of freedom pitch- and plunging model.

A great deal of research activity devoted to the aeroelastic active control and flutter suppression of flight vehicles has been accomplished. The two main fundamental objectives of flow control devices are: i) control of aeroelastic vibrations and ii) suppression of dynamic aeroelastic instabilities, such as flutter and non-linear LCOs. The state-of-the-art advances in these areas are presented by Dowell [2] in his latest edited monograph which discusses the current theoretical, computational and experimental research conducted in the field of nonlinear aeroelasticity. Within the aeroelastic experimentations conducted in the research community, the group led by Strganac at the University of Texas A&M has made major contributions and has extensively investigated nonlinear plunging and pitching aeroelastic models in low speed wind tunnel testing. A portion of their research has encompassed two wing sections with leading and trailing edge control surfaces used for aeroelastic suppression [2]. Block et al. [3] used a full-state feedback controller that demonstrated the ability to stabilize the nonlinear aeroelastic testing apparatus system at twice the open loop flutter velocity. Also, passive control techniques were explored by Hill et al. [4] that demonstrated a nonlinear energy sink device to be effective in increasing the overall stability threshold of the aeroelastic system. In recent years, several active linear and nonlinear control capabilities have been implemented. Digital adaptive control of a linear aeroservoelastic model, are only a few of the latest developed active control methods [5-7].

One class of active flow control devices that has garnered numerous theoretical and experimental investigations are zero net mass flow (ZNMF) actuators. ZNMF actuators are different from traditional controls such as flaps and spoilers in that they use no mechanical devices to directly alter the flowfield. Rao et al. [8] characterized electrical motor driven synthetic jet actuators (SJAs) using particle imaging velocimetry (PIV) in a water tunnel and showed the ability to delay separation on the airfoil. Furthermore, a piezoelectric actuator driven at 63.5 [Hz] was reported to produce a mere 1.87 [m/s] exit velocity when installed in a static wing configuration [8]. Many researches have improved the performance of piezoelectric SJAs, for example Gallas et al. [9], have shown that oscillating the piezoelectric membrane at its natural frequency can result in exit velocities between 30 and 50 [m/s].

The research performed at Clarkson University includes wind tunnel experiments for aeroelastic responses and the applicability of ZNMF actuators in active flow control schemes. The theoretical and numerical models proposed in previous research needs to be validated through experimental testing [10]. To compliment the numerical efforts an aeroelastic test apparatus was designed to accommodate the parameters defined by the aeroelastic characteristics of the prescribed wing section. The system has been designed for ease of use and adaptability for future installation of

active flow control devices that will be tested in an aeronautical low speed wind tunnel. The prescribed wing features a composite shell with a symmetric NACA 0018 profile. Due to the physical constraints of the wing it is considered to be rigid, with all the elastic properties concentrated in the springs and cam system. The constructed test apparatus is based on existing test beds developed at Texas A&M University and NASA Langley Research Center [4, 15]. The apparatus features independent pitch and plunge movement that will allow the wing to exhibit plunging pitching flutter and LCO at a certain frequency and dynamic pressure.

The rest of the paper is organized as follows. Section II contains preliminary calculations and modeling based on basic aeroelastic theory. Section III gives insight into the experimental setup. Section IV details the results of the experimental testing, and Section V discusses the control objective and planned experiments. Section VI summarizes the conclusions of the paper.

II. Preliminaries on the Aeroelastic Theory and Analytical Modeling

The aeroelastic system is modeled as a wing section that allows for two degrees of freedom. The wing section is mounted so that pitching and plunging are permitted as illustrated in Fig. 1. For this model the aeroelastic governing equations for the 2-DOF system can be written as follows [3,12,13]:

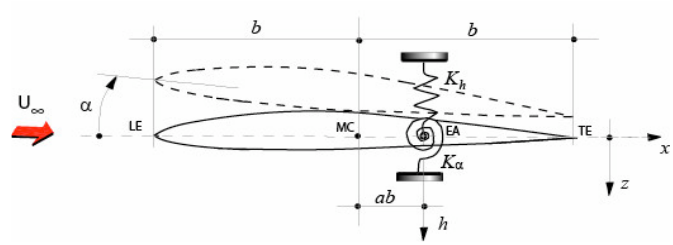

Figure 1: 2-DOF pitching and plunging wing section.

$$m\ddot{h} + mx_\alpha b\ddot{\alpha} + c_h\dot{h} + k_h h = -L(t) + L_d(t) + L_c(t) \tag{1}$$

$$I_\alpha\ddot{\alpha} + mx_\alpha b\ddot{h} + c_\alpha\dot{\alpha} + k_\alpha(\alpha)\alpha = M(t) + M_d(t) + M_c(t) \tag{2}$$

where the structural nonlinearities are retained in the equations of motion [15]. In equations (1) and (2) $L(t)$ and $M(t)$ are the aerodynamic lift and moment respectively; L_d and M_d are aerodynamic flow disturbances, such as gust loads, while L_c and M_c are the external loads due to the SJAs. The aerodynamic lift and moment in quasi-steady form that have been used in the analytical model are represented in equations (3) and (4).

$$L(t) = \rho_\infty U_\infty^2 b c_{l\alpha}\left[\alpha(t) + \frac{\dot{h}(t)}{U_\infty} + \left(\frac{1}{2} - a\right)b\frac{\dot{\alpha}(t)}{U_\infty}\right] \tag{3}$$

$$M(t) = b \cdot L(t) \tag{4}$$

In this preliminary analysis only linear quasi-steady aerodynamic loads have been considered, however modifications to include secondary effects and flow separations are also contemplated.

As in the actual test apparatus, the analytical model considers the plunging h and pitching α displacements to be restrained by springs with stiffnesses denoted as K_h and $K_\alpha(\alpha)$ and are attached at the elastic axis of the wing section. In this case, $K_\alpha(\alpha)$ represents the continuous nonlinear restoring moment in the pitch degree-of-freedom. The previous models have successfully produced analytical numerical solutions to the nonlinear coupled aeroelastic governing equations of motion [10,18]. However, authors have reported discrepancies between the experimental measurements and the analytical analysis [11]. These discrepancies can most likely be accounted for in the Coulomb damping forces that occur within the pitch bearing and plunge slider motion that is not taken into account in many of the models. At low velocities, damping is much greater than at higher velocities creating nonlinear

damping. Coulomb damping can be represented in the governing equations as a force opposing the motion of the system. A direct relationship exists between the damping and friction terms because the damping becomes negligible as soon as the friction force is greater then the restoring force. Thus the system can not experience aeroelastic oscillations when the restoring force is less then the friction and damping forces. When Coulomb damping is accounted for in the aeroelastic model, the equations for the plunge and pitch damping forces are as follows:

$$F_h = {}_h mg\left|\dot{h}\right|\dot{h}^{-1} \tag{5}$$

$$F_\alpha = {}_\alpha M_f\left|\dot{\alpha}\right|\dot{\alpha}^{-1} \tag{6}$$

Herein M_f is the frictional moment due to the nonlinear cam and ${}_h$, ${}_\alpha$ are the frictional coefficients, which can be determined for example by means of the decaying peak amplitudes [3]. In a straightforward manner, the aeroelastic governing equations (1) and (2) accounting for (5) and (6) can be converted into the equivalent state-space form, which is more suitable for the implementation of a control [1,14].

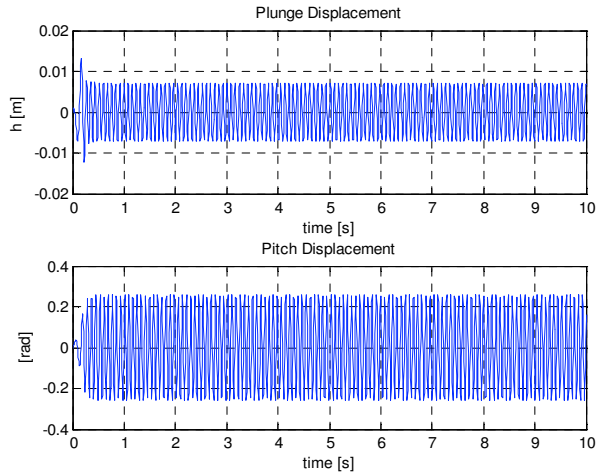

Figure 2: Analytical aeroelastic LCO response for quasi-steady aerodynamics.

III. Experimental Setup

Clarkson University Aeroelastic Test Apparatus

In this section, we describe our implementation of the test apparatus which was used to experimental characterize aeroelastic properties. Two similar test apparatus designed at NASA Langley and University of Texas A&M have aided researchers in developing their plunging-pitching devices and in characterizing the aeroelastic properties of such systems [14-17]. The ability to demonstrate suppression of aeroelastic instabilities such as LCO and flutter through ZNMF has necessitated the design and development of such aeroelastic apparatus.

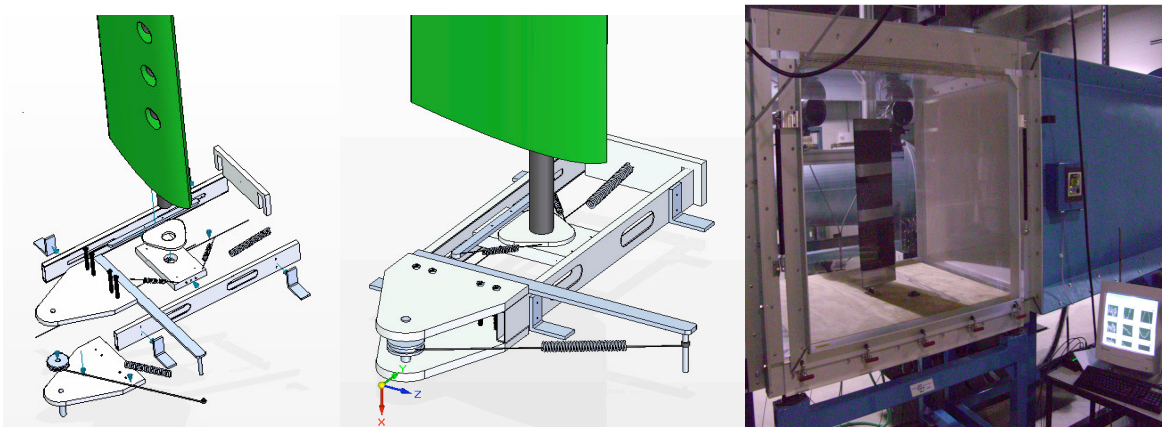

Figure 3: Exploded and assembled schematic of aeroelastic apparatus and installation in Clarkson University low speed wind tunnel.

Figure 3 schematically depicts the complete assembly of the 2-DOF test apparatus developed at Clarkson University. Such a design allows for independent pitching and plunging motions. To accomplish this kinematic

decoupling a bearing carriage system was utilized. The circular bearing, which allows for the pitch motion, is pressed into a carriage that is directly attached to the slider bearing allowing for motion in the plunge direction. Due to the large cantilevered nature of the wing, a considerable moment is translated through the bearing and onto the linear plunging system. A robust solution to help overcome the forces and keep the system from binding used slider drawer bearings rated for high moment loads. The nonlinear spring cam retention system shown in Fig. 3 is comprised of a nonlinear cam mounted to the rotational axis to restrict pitch movement and a linear cam mounted in line with the slider cart to restrict plunge displacement. The composite design of the wing is considered perfectly rigid within the parameters of our testing; therefore the elasticity of the system is inherently contained completely in the spring cam system. The main advantage of the system is that the springs connected to the cams as shown in Fig 3 are easily interchangeable allowing for parametric stiffness tests to be conducted. The initial static and dynamic tests will help to characterize the Coulomb damping coefficients c_h and c_α . Once the damping contributions have been characterized, these can be included in the analytical model to better investigate LCOs at low velocities. The parameters for the experimental apparatus are listed hereafter,

a =	-0.4	c_h =	$10.41 Nm^{-1}s^{-1}$	I_α =	$0.0032 kgm^2$	m_w =	$0.49 kg$
b =	$0.125 m$	$c_{l\alpha}$ =	$6.281/rad$	m_c =	$0.12 kg$	x_α =	$\left[0.0873-(b+ab)\right]/b$
c_α =	$.0126 Nm^{-1}s^{-1}$	$c_{m\alpha}$ =	$(0.5+a)c_{l\alpha}$	m_t =	$1.59 kg$		

The nonlinear pitch stiffness is related to the actual springs constant through the geometry of the cam and the attachment points, as schematically represented in Fig. 4. Using a coordinate transformation the tangential contact point for a given cam rotation can be determined; using the corresponding arm length the nonlinear restoring moment can be computed as a function of the pitch angle, and hence the stiffness can be derived. For the presented apparatus, the nonlinear restoring moment took on the 5th order polynomial form as follows:

$$k_\alpha(\alpha) = \sum_{i=1}^{5} \tau_i \alpha^{i-1} \tag{7}$$

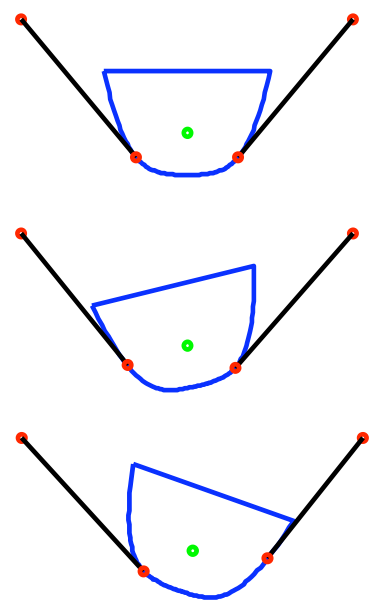

Figure 4: Nonlinear Cam

To accurately measure the aeroelastic response of the pitching-plunging apparatus accelerometers were mounted to the leading and trailing edge of the wing section shown in Fig. 5. The trailing edge and leading edge accelerometers are indicated by a_{TE} and a_{LE}, respectively; b_{TE} is the distance between the trailing edge and the elastic axis, b_{LE} is the distance between the leading edge and the elastic axis, θ is the angle caused by the leading edge geometry at the attachment of the accelerometer, and $\ddot{h}, \ddot{\alpha}$ are the wings plunging and pitching acceleration respectively.

$$a_{TE} = -b_{TE}\ddot{\alpha} + \ddot{h} \tag{8}$$

$$a_{LE} = \left(b_{LE}\ddot{\alpha} + \ddot{h}\right)\sin(\theta) \tag{9}$$

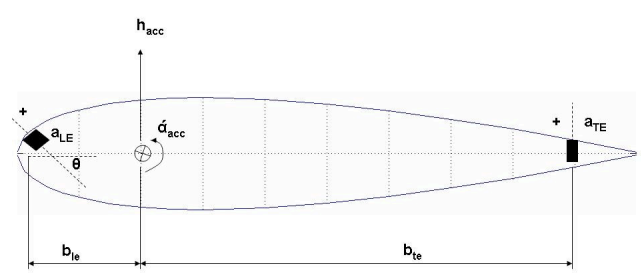

Figure 5: Schematic of wing mounted accelerometers

Equations (8) and (9) are solved for the pitching and plunging accelerations, $\ddot{\alpha}$ and $\ddot{h}$, respectively. The two accelerometers voltage outputs have been resolved into the pitching and

plunging motion about the elastic axis. To check the accuracy of the correlation an accelerometer was fixed to the apparatus carriage to directly measure the plunging acceleration. All of the voltage signals were converted to acceleration, velocities, and displacements were collected using LABVIEW© and recorded to a text output file that was post processed in MATLAB©.

IV. Experimental Results

The experimental data were used to obtain accurate damping terms. Coulomb damping is defined by a force restraining the motion of system, regardless of direction as shown in equations (5) and (6). In order to obtain the pitch and plunge damping terms independently, each free vibration case was run while locking down the other degree-of-freedom [3]. When the system is released into free vibration there is an inherent restoring force created by the springs in both the plunge and pitching degrees-of-freedom, this restoring force will keep the system in motion until the Coulomb damping and finally friction forces become greater then the overall restoring force. Recording the velocity time histories data for the free vibration case in Fig. 5, and associating the decaying peak amplitudes, a Coulomb damping model was created for analytical use. Cases were run for each spring set used in the experiment, the spring constants were 576, 604, 1186 [N/m] for sets 1,2,3 respectively. It is worth mentioning that Fig. 5 and 6 contain also the aerodynamic damping forces, since the wing section is attached to the system during the experiment. The resultant time history cases shown in Fig. 5 and 6 represented the total damping of the system. Therefore $_h$ and $_\alpha$ are given by the following:

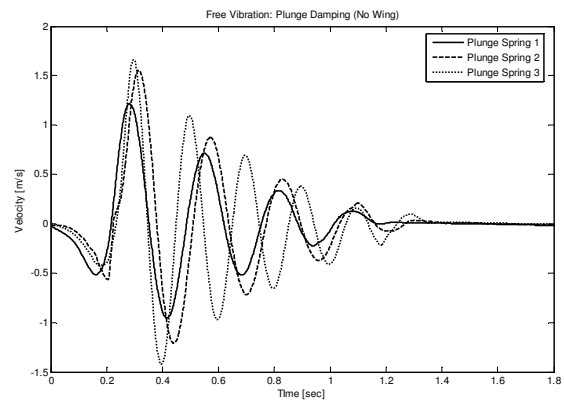

Figure 5: Free vibration response for different plunge spring constant

$$\mu_h = \frac{\Delta A_h}{4g}\omega_h^2 \tag{10}$$

$$\mu_\alpha = \frac{\Delta A_\alpha}{4g}\omega_\alpha^2 \tag{11}$$

here the decaying peak amplitudes are represented by ΔA of the free vibration cases [3]. This model was then compared to forced vibration case for two tunnel wind velocities of 5 and 6 [m/s] and plunge spring stiffness held constant at 1186 [N/m]. Fig. 6 represents the experimental forced vibration velocity versus time under-damped case for the system in the plunge direction. It can be observed that, as the system approaches the flutter boundary, the Coulomb damping becomes less important.

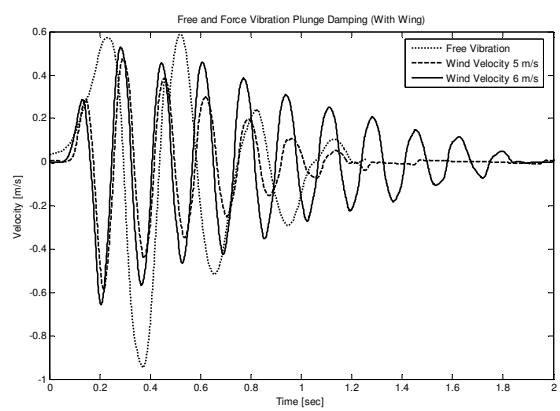

Figure 6: Free and forced vibration response for plunge spring stiffness k = 1186 [N/m], sub critical free stream velocity

A parametric study of varying plunge spring stiffness k_h was tested while holding constant the nonlinear pitch spring stiffness $k_\alpha(\alpha)$. During testing the free stream velocity U_∞ was started below the flutter boundary velocity and gradually stepped up until LCO or divergent flutter was reached.

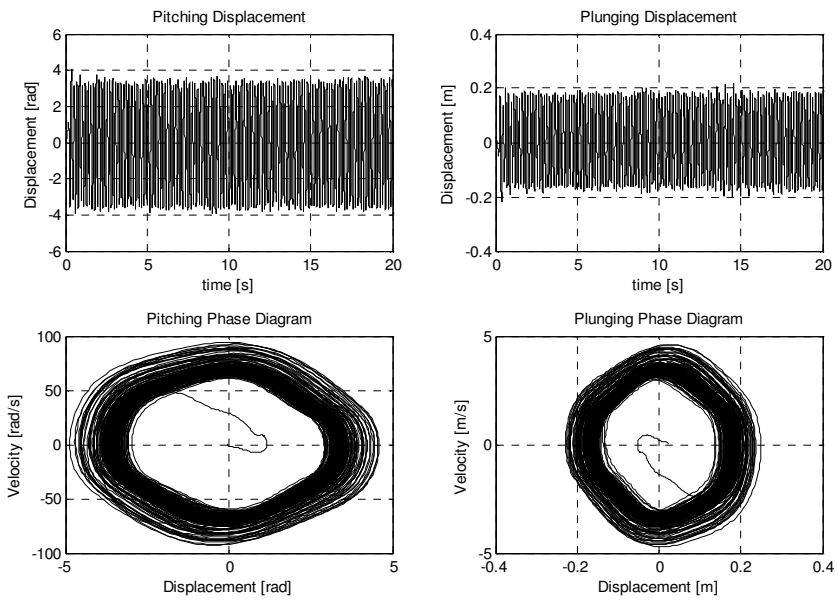

Figure 7: Time history and phase diagram for LCO response at 5 [m/s]

Figures 7 shows a typical stable LCO response for a plunge spring stiffness of 604 [N/m] and a free stream velocity of 5 [m/s]. The study showed that average LCO amplitudes varied from .085 to .175 [m] in the plunge direction and 5 to 15 [deg] of pitching rotation depending on the plunge spring stiffness. Also the LCO frequencies coalesced at values from 6 to 7.5 [Hz].

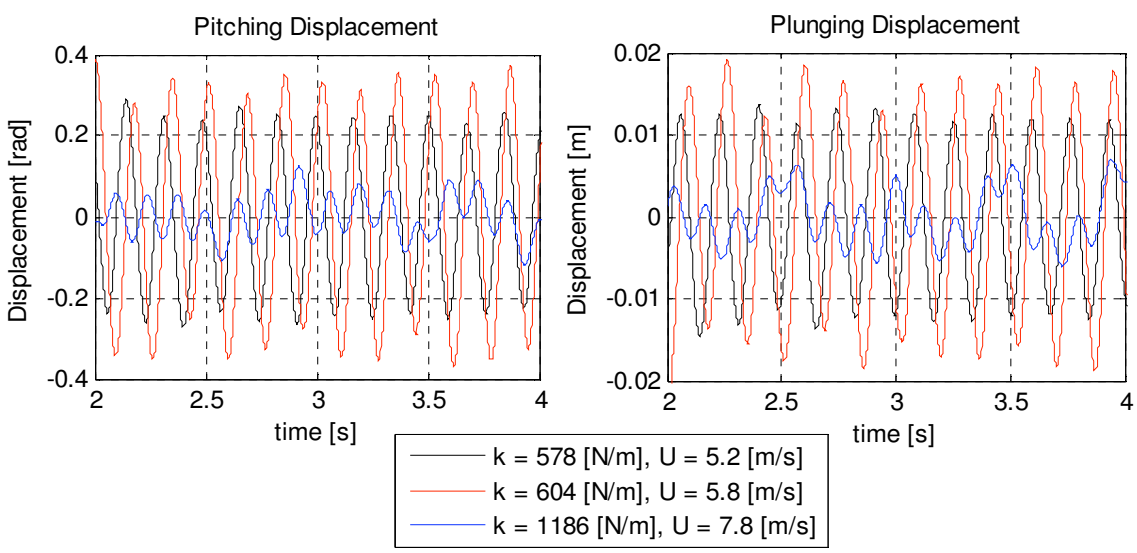

Figure 8: LCO responses for selected plunging spring stiffnesses (k)

Figure 8 graphically depicts the time history LCO response for the three plunge spring stiffness k_h cases. The first two cases show very similar LCO amplitudes and critical free stream velocities; this is most likely due to similar spring stiffness values.

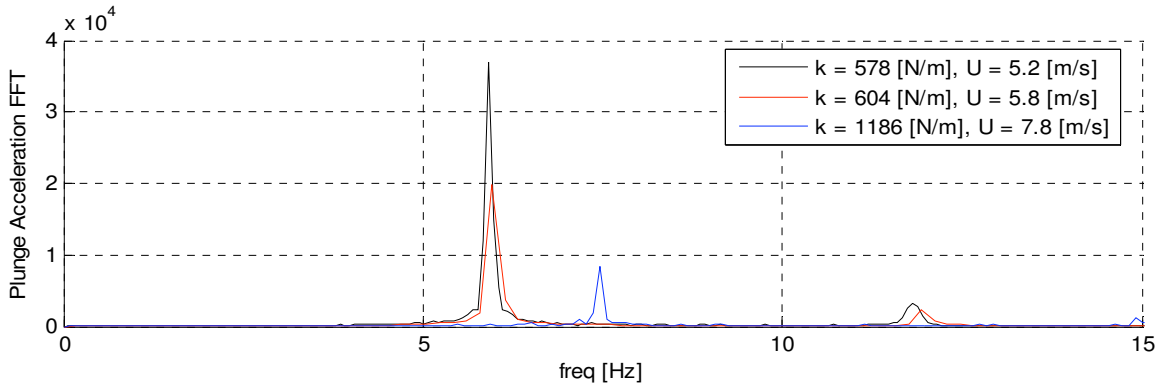

Figure 9: FFT of LCO response at selected plunging spring stiffness

When the k_h value was increased to 1186 [N/m] the stable LCO is obtained at 7.8 [m/s]. The corresponding FFT are graphically shown in Fig. 9. The results of Fig. 8 show that as k_h is increased the independent pitch and plunge motion frequencies coalesce at a larger value. Generally the experiment showed that a larger the plunge spring stiffness k_h resulted in smaller LCO amplitudes and higher frequencies.

Another means of characterizing the aeroelastic system is by exploring the bifurcation plots. Many bifurcation plots are represented in the form of LCO amplitude versus another system parameter such as wind tunnel velocity. By observing nonlinear bifurcations, aeroelastic responses can be determined in the vicinity of the flutter boundary. This nonlinear analysis can determine the LCO stability. In Fig. 9 a general bifurcation plot depicts two different LCO responses [1]. It can be clearly seen that when weakly nonlinearities are present in the aeroelastic system the LCO quickly reach large amplitude with a consequent divergent behavior. Conversely, strong nonlinearities create a more stable LCO response. To explore this phenomenon a second parametric study was conducted on the aeroelastic test apparatus. The investigation aided in exploration of the effects the nonlinear spring stiffness $k_\alpha(\alpha)$ and its interaction with the linear plunge spring k_h as shown in Fig. 11.

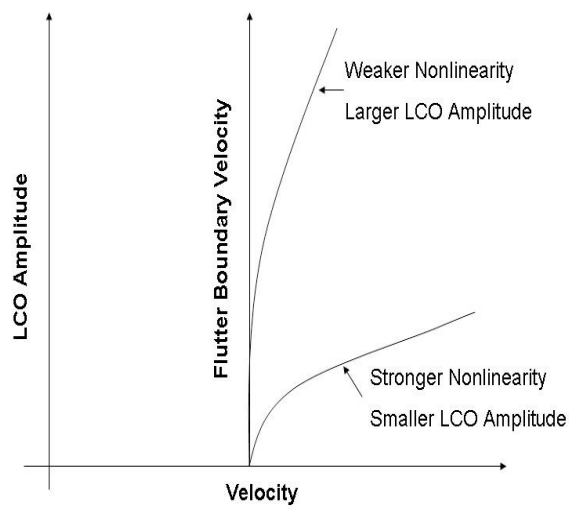

Figure 10: Bifurcation plot showing two main LCO characteristics

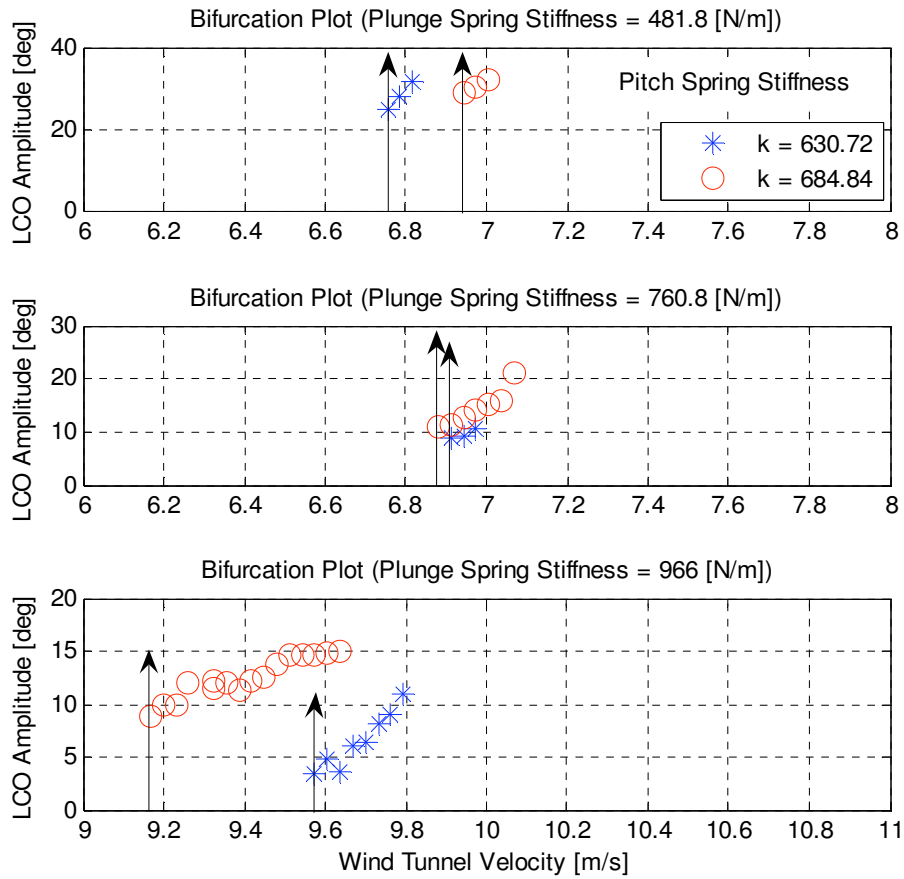

Figure 11: Bifurcation plots, arrows represent critical boundary velocity

The experimental data depicted in Fig. 11 give insight into the relationship of the nonlinear pitch and the linear plunge springs where the arrows represent the critical flutter boundary speed. The bifurcation plots show that for higher spring stiffness, both $k_\alpha(\alpha)$ and k_h, a stable LCO is maintained for a larger range of wind speeds. Also a general trend is witnessed between the plunge and spring stiffness relationship. The preliminary results show that for larger k_h the critical flutter boundary occurs at higher velocities for smaller $k_\alpha(\alpha)$ values. More exhaustive test will be conducted for a wider range of spring stiffnesses to aide in the full understanding of this phenomenon.

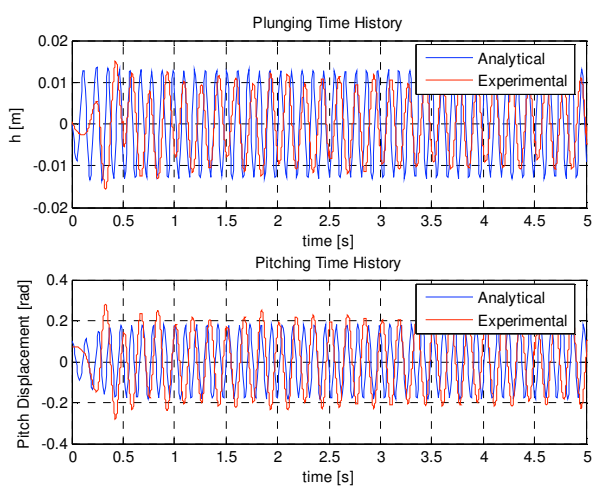

Figure 12: Analytical and Experimental response for plunge spring k = 604 [N/m] and free stream velocity = 5.8 [m/s]

On completion of the experimental parametric studies, the physical parameters of the apparatus were applied to the analytical quasi-steady aerodynamic model for qualitative comparisons. All the physical parameters of the system are given in the experimental setup section. The analytical model used the general equations of motion (1) and (2), with the aerodynamic loads of (3) and (4), rewritten in state-space form: a direct numerical integration has been performed with a Runge Kutta scheme, as implemented in the MATLAB© ODE45 solver. Fig. 12 graphically represents the comparison between experimentally recorded displacement time history and analytically computed displacement response for the same spring constants and free stream velocity. The analytical model shows a very good correlation with the experimental data in amplitude and a slight difference in frequency. These discrepancies are currently being investigated, in particular further analyzing the possible sources of uncertainties in the model, such as the overall compliance of the structure, mass unbalance, and other damping mechanisms. The validated analytical model will be used as a tool for control theory applications and within the formulation of the proper control laws. This research is on-going and preliminary results and discussions are presented in [10].

V. Application of ZNMF for Active Flow and Aeroelastic Control

A. Preliminaries on SJAs

Active flow and aeroelastic control are multidisciplinary research areas combining flow physics, sensing, control and actuation with the goal of changing the flowfield characteristics to enhance and increase the aerodynamic and structural performances [18]. The SJAs are in the class of ZNMF actuators because they require no input mass but produce a non-zero momentum output. The two basic components of and SJA are the cavity and the oscillating diaphragm schematically depicted in Fig. 13. The installation of SJAs will give the wing the capability to actively change its boundary layer. The altering of the boundary layer has enabled and proven that these devices can help drag reduction, lift enhancements, mixing augmentations and flow-induced noise suppression [21]. Promising research conducted by Duvigneau and Visonneau reported a stall delay from 16 to 22 [deg] and a increase in the maximum lift of +52% with respect to the baseline airfoil for optimal parameters [8]. The work previously conducted on optimization and the control parameters will be taken into consideration and implemented in the second phase of testing. To supplement the work being carried out at Clarkson University, the design and optimization of synthetic jets to be used in this research are being conducted in collaboration with Delft University of Technology, The Netherlands [10].

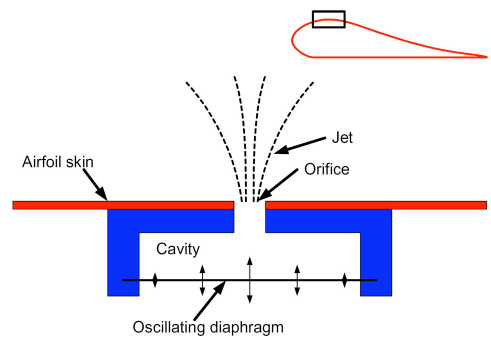

Figure 13: Schematic of synthetic jet actuator (SJA)

A. Synthetic Jet Actuation Future Experiments

A stereolithography NACA 0018 section (shown in Fig. 14) was designed to test and validate SJAs. The wing section incorporates internal pressure taps and can be mounted to a force balance to quantify the resulting difference between actuation and no actuation

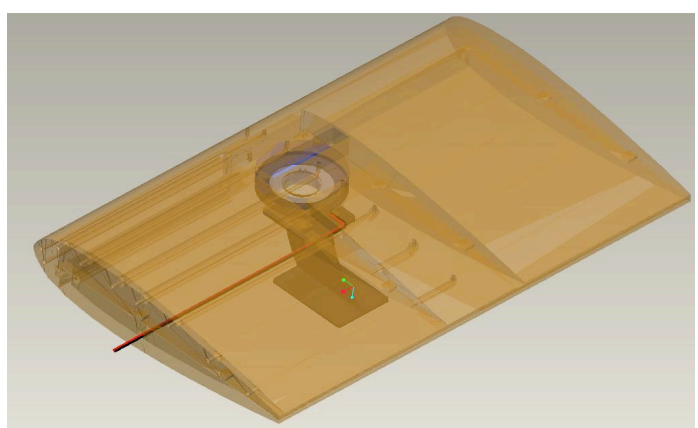

Figure 14: Schematic of sterolithography model with installed actuator, internal pressure tapings, and interchangeable orifices section.

for selected values of the angle-of attack and the actuation frequency of the SJA. The force balance has a manual crank to accurately change the angle-of-attack. A basic potentiometer circuit is used to vary the frequency of actuation.

Furthermore, two orifice designs will be tested. The first design will use a 1 mm exit hole diameter, while the second orifice will use a 1 mm slot running across the diameter of the actuator. Initial open-loop experiments can be used to develop a complete understanding of SJAs effects on boundary layer separation and on the unsteady aerodynamic lift and moment. After acquiring this experimental knowledge an accurate translation of the physics of SJAs to the computational domain can be made. Furthermore, a closed-loop control law can be developed and tested to study the performance of the SJAs in suppressing aeroelastic instabilities and enhance lifting surface performances.

VI. Concluding Remarks

A two-degree of freedom aeroelastic test apparatus has been designed, built and instrumented to aide in experimental investigations. Preliminary tests conducted in the Clarkson University low speed wind tunnel facility has shown that the nonlinear aeroelastic apparatus is capable of achieving flutter and LCOs. A parametric study was carried out to assess the effect of several linear and non-linear stiffnesses on the system. Low speed testing showed LCO plunging amplitudes from .015 to .04 [m] and pitching amplitudes from .1 to .35 [rad] with frequencies varying from 3 to 7.5 [Hz] depending on stiffness configurations. As a general trend, the aeroelastic system with larger stiffness exhibited the smaller amplitudes and higher frequencies LCO. Furthermore, a preliminary relationship between plunge and pitch spring stiffnesses was developed. More testing needs to be conducted to aide in the full understanding of the systems linear and non-linear stiffness and damping interactions. The experimental data was correlated with the developed analytical model that will help in the creation and implementation of active flow control schemes by mean of ZNMF. Finally, installed actuators will be tested on the aeroelastic apparatus with the ultimate goal of efficiently improving the overall aeroelastic performance of the system.

Acknowledgments

The authors would like to acknowledge partial support for this research from the MDA under contract # 375-36446, Clarkson University School of Engineering seed grant, the NSF-REU and McNair Programs for supporting Charles McNall summer internship.

References

1. Librescu, L., Marzocca, P., "Advances in the Linear/Nonlinear Control of Aeroelastic Structural Systems," *Acta Mechanica*, Vol. 178, No. 3-4, August 4, 2005, pp. 147-186..
2. Dowell, E.H., Clark, R., Cox, D., Curtiss, H.C Jr, Edwards, J. W., Hall, K. C., Peters, D. A., Scanlan, R., Simiu, E., Sisto, F., Strganac, T. W., *A Modern Course in Aeroelasticity*, Fourth Revised, Kluwer Academic publishers, copyright (2004).
3. Block, J. J., Gilliatt, H., "Active Control of an Aeroelastic Structure" AIAA, Aerospace Sciences Meeting & Exhibit, 35th, Reno, NV, Jan. 6-9, 1997. AIAA Paper 97-0016. *Texas A&M University, College Station, Texas, 77843-3141.*
4. Hill, W., Strganac, T., Nichkawde, C., "Suppression of Aeroelastic Instability with a Nonlinear Energy Sink: Experimental Results," *47th AIAA/ASME/ASCE/AHS/ASC Structures, Structural Dynamics, and Materials Conference*, 1-4 May 2006, Newport, Rhode Island.
5. Mukhopadhyay, V. (ed.), "Benchmark Active Control Technology," Pt. 2, *Journal of Guidance, Control, and Dynamics*, Vol. 23, No. 6, 2000, pp. 1093–1139.
6. Mukhopadhyay, V. (ed.), "Benchmark Active Control Technology," Pt. 3, *Journal of Guidance, Control, and Dynamics*, Vol. 24, No. 1, 2001, pp. 146–192.
7. Mukhopadhyay, V., "Historical Perspective on Analysis and Control of Aeroelastic Responses," *Journal of Guidance, Control, and Dynamics*, Vol. 26, No. 5, 2003, pp. 673–684.
8. Rao, P.P., Strganac, T.W., Rediniotis, O. K., "Control of Aeroelastic Response Via Synthetic Jet Actuators," *41st AIAA/ASME/ASCE/AHS/ASC Structures, Structural Dynamics, and Materials Conference*, AIAA 2000-1415, Atlanta, GA, 3-6 April 2000.
9. Gallas, Q., Holman, R., Toshikazu, N., Carroll, B., Sheplak, M., Cattafesta. L., "Lumped Element Modeling of Piezoelectric-Driven Synthetic Jet Actuators," *AIAA Journal*, Vol 41, No. 2, February (2003).
10. O'Donnell, K., Schober, S., Stolk, M., Marzocca, P., De Breuker, R., Abdalla, M., Nicolini, E., Gurdal, Z., "Active Aeroelastic Control Aspects of an Aircraft Wing by Using Synthetic Jet Actuators: Modeling, Simulations, Experiments," The 14th International Symposium on: Smart Structures and Materials & Nondestructive Evaluation and Health Monitoring, SPIE 6523-8, San Diego, CA, 18-22 March 2007.
11. Duvignequ, R., Visonneau, M., "Optimization of a Synthetic Jet Actuator for Aerodynamic Stall Control," Elsevier, *Laboratorire de Mecanique des Fluides CNRS UMR 6598, Ecole Centrale de Nantes, B.P. 92101, rue de la Noe FR-44321, Nantes cedex 3, France,* 13 January 2005.
12. Block, J.J., Strganac, T.W., "Applied Active Control for a Nonlinear Aeroelastic Structure" *Journal of Guidance, Control, and Dynamics*, Vol. 21, No.6, pp. 838-845 (1998).
13. C. Rubillo, P. Marzocca, E. Bollt, "Active Aeroelastic Control of Lifting Surfaces via Jet Reaction Limiter Control," *International Journal of Bifurcation and Chaos*, Vol. 16, No. 9, 2006, 2559–2574.
14. O'Neil, T., Experimental and Analytical Investigations of an Aeroelastic Structure with Continuous Nonlinear Stiffness, *Texas A&M University Masters of Science Thesis*, May 1996.
15. O'Neil, T., Straganac, T.W., Aeroelastic Response of Wing Supported by Nonlinear Springs, *Journal of Aircraft*, Vol. 35, No. 4, July-August 1998.
16. O'Neil, T., Gilliatt, H., Strganac, T. W., Investigations of aeroelastic response for a system with continuous structural nonlinearities, AIAA, ASME, AHS, and ASC, 37th, Structures, Structural Dynamics and Materials Conference, Salt Lake City, UT, Apr. 18, 19, 1996.
17. O'Neil, T., Nonlinear aeroelastic response – Analyses and Experiments, AIAA, Aerospace Sciences Meeting and Exhibit, 34th, Reno, NV, Jan 15-18, 1996.
18. Behal, A., Marzocca, P., Rao, V. M., Gnann, A., Nonlinear Adaptive Control of an Aeroelastic Two-Dimensional Lifting Surface, *Journal of Guidance Control and Dynamics*, Vol. 29, No. 2, March-April 2006.
19. Utturkar, Y., Holman, R., Mittal, R., Carroll, B., Sheplak, M., Cattafesta L., A jet Formation Criterion for Synthetic Jet Actuators, 41st Aerospace Sciences Meeting & Exhibit, 6-9 January 2003/ Reno, NV.
20. Kerschen, G., Lee, Y. S., Vakais, A. F., McFarland, D. M., Bergman, L. A., Irreversible Passive Energy Transfer in Coupled Oscillators with Essentials Nonlinearity, SIAM J. Appl Math, Vol. 66, No 2, pp. 648-679.
21. Lee, C., Hong, G., Ha, Q. P., Mallinson, S. G., A piezoelectrically actuated micro synthetic jet for active flow control, Elsevier, Finale Paper accepted, 12 May 2003.
22. McFarland, D. M., Kerschen, G., Kowtko, J. J., Lee, Y. S., Bergman, L. A., Vakais, A. F., Experimental Investigation of targeted energy transfers in strongly and nonlinearly coupled oscillators, J. Acoust. Soc. Am., 118(2), August 2005.

23. Traub, L. W., Miller, A., Rediniotis, O., Effects of Active and Passive Flow Control on Dynamic-Stall Vortex Formation, Journal of Aircraft, Vol. 41, NO.2: Engineering Notes.
24. Waszak, M., Modeling the Benchmark Active Control Technology Wind-Tunnel Model for Application to Flutter Suppression, AIAA Paper No. 96-3437. AIAA Atmospheric Flight Mechanics Conference. San Diego, CA. July 29-31, 1996..
25. Dowell, E.H., Edwards, J., and Strganac, T., "Nonlinear Aeroelasticity," *Journal of Aircraft*, Vol. 40, No. 5, 2003, pp. 857–874.